Systematic development of *ab initio* tight-binding models for hexagonal metals

J. Smutna, R. M. Fogarty, M. R. Wenman, and A. P. Horsfield*

Department of Materials and Thomas Young Centre, Imperial College London, South Kensington Campus, London SW7 2AZ, United Kingdom

(Received 1 January 2020; accepted 9 March 2020; published 10 April 2020)

A systematic method for building an extensible tight-binding model from *ab initio* calculations has been developed and tested on two hexagonal metals: Zr and Mg. The errors introduced at each level of approximation are discussed and quantified. For bulk materials, using a limited basis set of *spd* orbitals is shown to be sufficient to reproduce with high accuracy bulk energy versus volume curves for fcc, bcc, and hcp lattice structures, as well as the electronic density of states. However, the two-center approximation introduces errors of several tenths of eV in the pair potential, crystal-field terms, and hopping integrals. Environmentally dependent corrections to the former two have been implemented, significantly improving the accuracy. Two-center hopping integrals were corrected by taking many-center hopping integrals for a set of structures of interest, rotating them into the bond reference frame, and then fitting a smooth function through these values. Finally, a pair potential was fitted to correct remaining errors. However, this procedure is not sufficient to ensure transferability of the model, especially when point defects are introduced. In particular, it is shown to be problematic when interstitial elements are added to the model, as demonstrated in the case of octahedral self-interstitial atoms.

DOI: 10.1103/PhysRevMaterials.4.043801

I. INTRODUCTION

Atomistic simulations of most hexagonal metals and their alloys have been dominated by two classes of models: density functional theory (DFT) [1] and classical empirical potentials [most notably embedded atom model (EAM) [2]]. DFT models are effectively parameter free and transferable for use over a large range of different systems [3]; however, they are severely limited by the computational resources required for a simulation, with system sizes only rarely exceeding 1000 atoms [4–6]. Empirical potentials, on the other hand, require extensive parametrization, which may need to be redone with the addition of new elements to the model, and are generally only applicable for a limited number of problems. For instance, the Mendelev and Ackland EAM potentials for Zr have one parametrization for reproducing the phase transition from hcp to bcc and another for modeling defects in hcp Zr [7]. The empirical potentials also often exclude important physical effects (such as charge transfer in the case of EAM), which can result in poor accuracy when modeling chemical reactions [8]. Due to the increasing recognition of the practical importance of understanding complex phenomena, there is a clear demand for models capable of accurate simulations involving multiple atomic species and large numbers of atoms (many thousands or more).

Tight-binding (TB) models lie on the boundary between DFT and empirical potentials. They include an explicit representation of electronic structure, and therefore bond formation, but are calculated in a more approximate (and therefore faster) way than in DFT [9–17]. The use of a minimal basis set of atomic orbitals means TB models are not an obvious choice for free-electron-like metals. However, we find that using a basis set of *s*, *p*, and *d* orbitals is sufficient for many properties of hexagonal metals and alloys. Note that the full overlap matrix must be retained as there is significant overlap of orbitals on neighboring sites.

In two-center TB, the numerical values of the integrals describing each interaction can be precalculated before a simulation, as they only depend on the distance and orientation of two orbitals, significantly improving the speed of subsequent simulations [10,16,18,19]. However, for solids this is a significant approximation as three-center terms can be important [12,14,20]. There is a range of methods for obtaining the values of the required integrals. Semiempirical TB requires the value of each of these integrals to be fitted to accurate data (often found from DFT) in order to reproduce the electronic states up to the Fermi level, the binding energies, and the forces [9,10,18,21–26]. Since the calculation of the electronic states involves a diagonalization of the entire Hamiltonian matrix, all the integrals need to be fitted at the same time. The more complex the underlying TB model (both in terms of features included and number of atomic orbitals considered), the larger the number of parameters required to describe the variation of these integrals with distance, and the higher the risk of not finding optimal values or overfitting. Moreover, a large data set of DFT calculations is generally required as target for this optimization [19,22,24]. In the end, these methods have many of the same advantages as empirical potentials, but also suffer from some of the same problems. There can be a lack of transferability as they often need to be refitted when adding new elements.

Another way to obtain the parameters is by calculating the values of the integrals required directly [12,14,16]. Density functional tight binding (DFTB) uses a more systematic approach based on full DFT calculations of the on-site energies, hopping, and overlap for a dimer; crystal-field integrals are sometimes also included [22]. A pair potential (often treated

*a.horsfield@imperial.ac.uk

as purely repulsive) is then fitted to incorporate the ion-ion interactions and to approximately compensate for missing electron repulsion and the many-center interactions [16]. Again, target data from a more reliable calculation is needed, but this time only energies and forces are required (not the electronic structure) and fitting of a pair potential is much simpler. This approach works well as long as the many-center interactions do not have a significant effect on the electronic structure, and has been successful in modeling many molecular systems, and other open structures [16].

This method has been improved by the group of Cawkwell using the tabulated DFTB values as a starting point, followed by numerical optimization of the integrals for the electronic structure to correct for many-center effects. This method gives rise to models for molecules involving C, H, N, and O with high accuracy in the predicted bond lengths and binding energies [19]. Starting from a reasonable guess of parameters reduces the demands on the optimization step in the process and reduces the risk of overfitting.

The main disadvantage of all methods where terms are dropped and compensated for by fitting is the lack of transparency of the different sources of error. When modeling systems where many-center interactions are important, for example, an interstitial defect in a close-packed metal, it is hard to predict the performance of a particular TB model and the error due to the approximations. As a result, it is difficult to predict the suitability of a TB model for a given simulation or even material, and predict which physical phenomena might be causing the model to fail. Establishing the reasons for errors, and hence what needs to be done to correct them, is one of the aims of this work.

Another more recent class of TB models worth mentioning takes a more systematic approach to obtaining two-center hopping integrals directly from DFT simulations of periodic systems [23,27–29]. This approach mainly focuses on the hopping integrals for particular perfect crystal systems with one or two elements, and does not address the question of transferability for metals with defects. However, for defects and dislocations in silicon it has been found that many-center interactions can be too large for a two-center model to be suitable [30].

The approach taken here to building a two-center TB model involves four steps: selection of an appropriate basis set; tabulation of the two-center overlap, hopping, and crystal-field integrals as well as an initial pair potential using the DFTB approach; the application of many-center corrections for each of these terms; and pair-potential fitting. For the crystal field and the pair potential, an embedding term based on the electron density overlaps is used. Fitting directly to DFT integrals [23] (as opposed to band structure) is used to correct the hopping integrals; a pair potential is subsequently fit to reproduce plane-wave structural results. The errors introduced in each step of the approximation are evaluated for both perfect crystals and defects.

Our choice of metals used in the analysis of TB is governed by our interest in corrosion. Corrosion is a complex process that can only be simulated at the atomic scale by methods that treat electrons explicitly. DFT has been employed, but TB might enable a deeper understanding to be acquired as its computational efficiency enables larger numbers of atoms and longer timescales to be reached. However, the models need to be robust. Here, we look at TB models for two materials for which corrosion is a key concern at the present: Zr and Mg. Cladding of of water-cooled nuclear reactor fuel currently uses Zr alloys; consequently, understanding the corrosion behavior of its alloys under irradiation is of current importance to the nuclear industry. Systems beyond the size attainable by traditional plane-wave DFT are needed to model the defects introduced by the radioactive environment and their interaction with the alloying elements, as well as their influence of the corrosion rate and hydrogen pickup [31,32]. Mg is the lightest structural metal available, and thus could be used to reduce fuel consumption by making trains, planes, and cars lighter. However, it is prone to corrosion, and our understanding of what happens when it corrodes is far from complete [33].

II. TB FORMALISM

A. Harris-Foulkes DFT

The first approximation central to all TB models is the use of a basis set of atom-centered orbital wave functions $\phi_{I\alpha}(\vec{r})$ to represent the electron wave functions, and hence the density $n(\vec{r})$, of the system. The molecular orbitals of the system are expanded in this set of atomic orbitals $\phi_{I\alpha}$,

$$\psi_p(\vec{r}) = \sum_{I\alpha} c_{p,I\alpha}\phi_{I\alpha}(\vec{r}), \tag{1}$$

where $c_{p,I\alpha}$ is an expansion coefficient, I is an index that runs over the atoms, and α indexes the atomic orbitals on each atom. The density is then computed from the molecular orbitals

$$n(\vec{r}) = \sum_p f_p|\psi_p(\vec{r})|^2, \tag{2}$$

where f_p is the occupancy of molecular orbital ψ_p. The total energy of the system is then given by the Kohn-Sham energy:

$$E[n] = \sum_p f_p \int \psi_p^*(\vec{r})\left(-\frac{\hbar^2}{2m}\nabla^2\right)\psi_p(\vec{r})\,d\vec{r} + E_{\text{Hartree}}[n] + E_{\text{ext}}[n] + E_{\text{xc}}[n], \tag{3}$$

where the first term is the kinetic energy, with $\hbar$ being Planck's constant, m the mass of an electron, E_{Hartree} the average electron-electron repulsion, E_{ext} the electron-ion and ion-ion interaction energies, and E_{xc} the exchange and correlation energy. The ground-state electronic energy is then calculated by finding the coefficients $c_{p,I\alpha}$ that minimize the Kohn-Sham energy.

Now, the Hohenberg-Kohn energy (which is equal to the Kohn-Sham energy for a given electron density) can be expanded in powers of $q(\vec{r}) = n(\vec{r}) - n^{(0)}(\vec{r})$ where $n^{(0)}$ is some

reference electron density:

$$E[n] = \underbrace{E[n^{(0)}]}_{E_0} + \underbrace{\int \left.\frac{\delta E}{\delta n(\vec{r})}\right|_{n^{(0)}} q(\vec{r})d\vec{r}}_{E_1} + \underbrace{\frac{1}{2}\iint \left.\frac{\delta^2 E}{\delta n(\vec{r})\delta n(\vec{r}')}\right|_{n^{(0)}} q(\vec{r})q(\vec{r}')d\vec{r}\,d\vec{r}'}_{E_2} + \cdots \quad (4)$$
$$= E_0 + E_1 + E_2 + \cdots .$$

The closer $n^{(0)}$ is to the ground-state electron density of the system studied, the smaller the higher-order terms are, and the more accurate low-order approximations to the final energy are.

The sum of atom-centered spherical electron densities $n_I(\vec{r})$ is used as the reference density: that is, $n^{(0)} = \sum_I n_I$ where I runs over the atoms. In this case, the individual terms in the energy expansion have a clear physical meaning. The first term E_0 corresponds to the energy of collections of atoms in the absence of electronic relaxation; this is similar in content to a Lennard-Jones potential. The second term E_1 corresponds to the charge redistribution associated with the formation of covalent bonds, i.e., the first-order electronic structure contribution; this becomes clearer when expressed in terms of atomic orbitals as shown below. The third term E_2 becomes important when significant charge transfer occurs in the system, as happens when atoms with very different electronegativities are present. In this paper we will mainly focus on E_0 and E_1 as charge transfer between atoms in pure metals without defects is relatively small. However, E_2 can become important when defects or additional elements are present. In the rest of this section, E_2 and higher-order terms will be neglected. Note that terms higher than E_2 are purely from the exchange and correlation energy.

For a given $n^{(0)}$, E_0 can be calculated simply by evaluating Eq. (3), where everything except the exchange and correlation can be represented exactly as a sum of one- and two-center integrals. Now, the ground-state density corresponds to the value of $q(\vec{r})$ that minimizes the total energy. Thus, if we neglect E_2 and higher terms, we can can find the corresponding ground-state density by making E_1 stationary. However, the resulting energy will not necessarily be above the true minimum [11,13,34]. Note that to perform this variational calculation we need to evaluate the different energy contributions. Using the Kohn-Sham expression for E_1,

$$E_1 = \sum_{I\alpha,J\beta} H^{(0)}_{I\alpha,J\beta}\left(\rho_{I\alpha,J\beta} - \rho^{(0)}_{I\alpha,J\beta}\right), \quad (5)$$

where $\rho_{I\alpha,J\beta} = 2\sum_n f_n c^*_{n,I\alpha} c_{n,J\beta}$ is the density matrix, n labels the eigenstates of $H^{(0)}_{I\alpha,J\beta}$, the factor of 2 accounts for spin degeneracy, $\rho^{(0)}_{I\alpha,J\beta}$ is the density matrix for the free atoms, and the Hamiltonian matrix is given by

$$H^{(0)}_{I\alpha,J\beta} = \int \phi_{I\alpha} \left.\frac{\delta E}{\delta n(\vec{r})}\right|_{n^{(0)}} \phi_{J\beta}\, d\vec{r}$$
$$= \int \phi_{I\alpha}(\hat{T} + V_{KS}[n^{(0)}])\phi_{J\beta}\, d\vec{r}, \quad (6)$$

where $\hat{T} = -\frac{\hbar^2}{2m}$ is the kinetic energy operator, and $V_{KS}[n,\vec{r}] = \frac{\delta E_{\mathrm{HXC}}[n]}{\delta n(\vec{r})}$ is the Kohn-Sham potential, and $E_{\mathrm{HXC}} = E_{\mathrm{Hartree}} + E_{\mathrm{ext}} + E_{\mathrm{xc}}$. The eigenstates of $H^{(0)}_{I\alpha,J\beta}$ are found from

$$\sum_{J\beta} H^{(0)}_{I\alpha,J\beta} c_{n,J\beta} = \epsilon_n \sum_{J\beta} S_{I\alpha,J\beta} c_{n,J\beta}, \quad (7)$$

where ϵ_n is the eigenvalue for state n. The matrix elements of $H^{(0)}$ are referred to as hopping integrals if $I \neq J$, and on-site terms (formed from an atomic contribution and crystal-field integrals) if $I = J$. The overlap matrix is defined by

$$S_{I\alpha,J\beta} = \int \phi_{I\alpha}\phi_{J\beta}\, d\vec{r}. \quad (8)$$

Just as for E_0, everything except the exchange and correlation part of the hopping and crystal-field integrals can be evaluated exactly as a sum of one-, two-, or three-center integrals.

B. Basis-set generation

The discussion that follows presupposes the use of an atomic basis set. Here, we describe how we build these basis sets. The reference electron density for each atom is formed from the filled atomic orbitals of a free atom. For instance, for Zr we use a $5s^2\ 4d^2\ 5p^0$ configuration, and so only the $5s$ and $4d$ orbitals contribute to the density, and hence to E_0. All orbitals contribute to E_1 as electronic relaxation causes mixing between orbitals. Atomic orbitals optimized for a solid will generally be less extended than ones for a free atom, thus the basis set is computed using an atom in a confinement potential of the form [35]

$$V_{\mathrm{conf}}(r) = V_0\left(\frac{r}{r_0}\right)^n, \quad (9)$$

with $V_0 = 2$ Ry and $n = 6$ [14]. The effect of this confining potential on the orbitals of Zr is shown on Fig. 1. The orbitals are constrained to zero at a radius $r_{\mathrm{cut}} > r_0$. The value for r_0 is varied to obtain a basis set that gives properties comparable

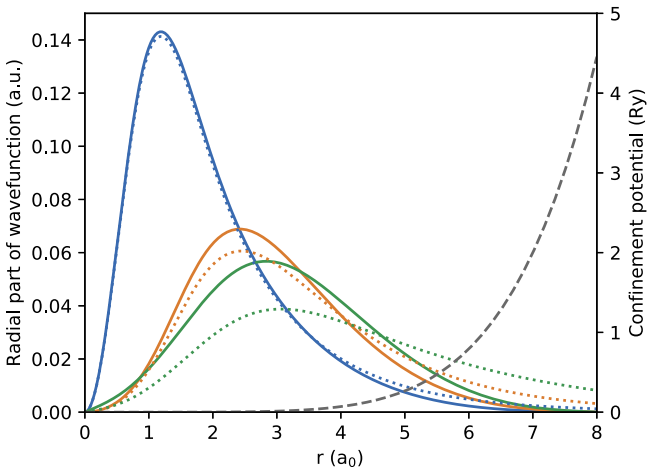

FIG. 1. The effect of the confinement potential with $r_0 = 7.0a_0$ and $r_c = 8.0a_0$ (dashed line) on the atomic orbitals (solid line) compared to those for a free atom (dotted line). In Zr, the $4d$ orbitals (blue) are almost unchanged, while the shape of the longer-ranged $5s$ (orange) and especially $5p$ (green) orbitals changes significantly.

to a more complete plane-wave basis-set calculation, notably, the correct equilibrium lattice parameters, energy ordering of different structures at equilibrium, and electronic density of states. It is possible to vary n, or even use a different confinement potential for each atomic shell; however, simply varying r_0 has often been found to be sufficient [12,36–38]. The range of the chosen basis set influences the computational cost: longer-range basis sets mean more integrals need to be calculated, and hence lead to slower calculations. Therefore, we wish to choose the shortest-range basis set possible that leads to reasonable properties. Unless stated otherwise, all calculations in this paper use a single-ζ *spd* basis set.

The evaluation of the integrals needed to calculate the different components of the energy is made more efficient by expanding each atomic orbital and pseudopotential in a series of Gaussian functions, a technique widely used in chemistry DFT codes. The pseudopotentials used here are the Goedecker type used in the CP2K code [39–41], which are formed from Gaussian functions. This allows all integrals needed to describe the kinetic energy, overlap matrix, and electrostatic interactions to be evaluated analytically; only the exchange and correlation integrals need to be computed numerically.

For Mg we used the GTH-PBE-q2 pseudopotential for which 10 electrons per atom were represented with a pseudopotential. For Zr we used the GTH-LDA-q4 pseudopotential. The choice was mainly motivated by the desire for a small basis set: the available PBE pseudopotentials for Zr include semicore $4s$ and $4p$ states, that do not directly contribute to bonding. The inaccuracies introduced by the use of this local density approximation (LDA) pseudopotential mainly manifest in calculations of self-interstitial defect formation energies, as discussed below. The Perdew-Burke-Ernzerhof (PBE) exchange and correlation functional is used throughout; it has been shown to reproduce well the physical properties of Mg and Zr alloys, including correctly predicting the lowest-energy site for interstitial H in Zr [42]. We now consider the approximations we make to the linear-combination-of-atomic-orbitals (LCAO) DFT calculations to further improve efficiency.

C. Two-center TB

In two-center TB we calculate all relevant quantities as a sum of pairwise contributions. The pairwise approximation to E_0 corresponds to a low-order cluster expansion, given by

$$E^0_{\rm coh} = E\left[\sum_I n_I\right] \approx \sum_I E[n_I] + \frac{1}{2}\sum_{I\neq J}(E[n_I+n_J]-E[n_I]-E[n_J]). \tag{10}$$

This has the form of atomic terms plus a pair potential, which can be tabulated as a function of distance between two atoms. The error in the pair potential is solely a result of exchange and correlation.

Matrix elements of the Kohn-Sham potential can also be approximated using a cluster expansion, giving

$$\int \phi_{I\alpha} V_{ks}\left[\sum_K n_K\right]\phi_{J\beta}\,d\vec{r} \approx \begin{cases} \int \phi_{I\alpha} V_{KS}[n_I+n_J]\phi_{J\beta}\,d\vec{r}, & I\neq J \\ \sum_K \int \phi_{I\alpha} V_{KS}[n_K]\phi_{I\beta}\,d\vec{r}, & I=J. \end{cases} \tag{11}$$

This allows the integrals to be computed from a set of precalculated tables, which leads to rapid building of the Hamiltonian. For crystal-field terms ($I=J$), all the errors arise from many-center effects in the exchange and correlation potential. For hopping terms ($I\neq J$) there are errors both from neglect of three-center neutral atom potential terms and the exchange and correlation terms.

D. A many-center correction for E_0

The many-center cluster expansion for $E_{\rm xc}[n^{(0)}]$ can be written as

$$E_{\rm xc}\left[\sum_I n_I\right] = \sum_I E_{\rm xc}[n_I] + \frac{1}{2}\sum_{I\neq J}(E_{\rm xc}[n_I+n_J] - E_{\rm xc}[n_I] - E_{\rm xc}[n_J]) + \Delta E_{\rm xc}, \tag{12}$$

where $\Delta E_{\rm xc}$ is the correction term we need. To estimate this correction we employ the approximation of Sankey and Niklewski [12], namely, that the exchange and correlation energy per particle varies slowly in space. This allows us to include multisite terms approximately, but in a computationally efficient way. Unfortunately, it is currently limited to the local density approximation (LDA). In the LDA we have

$$E^{\rm LDA}_{\rm xc}\left[\sum_I n_I\right] = \sum_I \int n_I(\vec{r})\epsilon_{\rm xc}\left(\sum_J n_J(\vec{r})\right)d\vec{r}, \tag{13}$$

where $\epsilon_{\rm xc}$ is the exchange and correlation energy per electron for a uniform electron gas. We now perform a Taylor expansion of $\epsilon_{\rm xc}(n)$ about an average value $\bar{n}_I$ to get

$$E^{\rm LDA}_{\rm xc}\left[\sum_I n_I\right] = \sum_I \int n_I(\vec{r})\left[\epsilon_{\rm xc}(\bar{n}_I) + \epsilon'_{\rm xc}(\bar{n}_I) \times\left(\sum_J n_J(\vec{r}) - \bar{n}_I\right) + \cdots\right]d\vec{r}. \tag{14}$$

If we let $Z_I = \int n_I(\vec{r})\,d\vec{r}$, $\bar{n}_{I,J} = \frac{1}{Z_I}\int n_I(\vec{r})n_J(\vec{r})d\vec{r}$, and $\bar{n}_I = \sum_J \bar{n}_{I,J}$, then Eq. (14) simplifies to

$$E^{\rm LDA}_{\rm xc}\left[\sum_I n_I\right] \approx \sum_I Z_I \epsilon_{\rm xc}(\bar{n}_I). \tag{15}$$

We can tabulate $\bar{n}_{I,J}$, allowing for efficient evaluation of Eq. (15).

Substituting Eq. (15) into Eq. (12) we get

$$\Delta E_{\rm xc} \approx \sum_I \Delta E_{{\rm xc},I}, \tag{16}$$

where

$$\Delta E_{\mathrm{xc},I} \approx Z_I \epsilon_{\mathrm{xc}}[\bar{n}_I] - Z_I \epsilon_{\mathrm{xc}}[\bar{n}_{I,I}] - \frac{1}{2}\sum_{J(\neq I)} Z_I[\epsilon_{\mathrm{xc}}(\bar{n}_{I,I}+\bar{n}_{I,J}) - \epsilon_{\mathrm{xc}}(\bar{n}_{I,I}) - \epsilon_{\mathrm{xc}}(\bar{n}_{I,J})].$$

We will refer to this as the uniform density correction.

E. Correcting crystal-field terms

Two-center crystal-field terms would be exact if it were not for their neglect of many-center exchange and correlation terms. We note that crystal-field terms not only affect the diagonal terms (by shifting the on-site energies), but can also produce nonzero off-diagonal terms, allowing hopping of an electron between two orbitals on the same atom. In practice, many of the off-diagonal contributions either cancel out due to the symmetry of the lattice, as is the case for cubic lattices, or are much smaller than the diagonal terms, as is the case for hcp lattices. Thus, we focus on just the diagonal terms.

If v_{xc} varies slowly in space, using a Taylor expansion, we can expand around an effective density value ($\bar{n}_{I\alpha J\beta}$) for the generic matrix element $v_{\mathrm{xc},I\alpha J\beta}$:

$$v_{\mathrm{xc},I\alpha J\beta}[n^{(0)}] \approx \int \phi_{I\alpha}(\vec{r})[v_{\mathrm{xc}}[\bar{n}_{I\alpha J\beta}] + v'_{\mathrm{xc}}[\bar{n}_{I\alpha J\beta}](n^{(0)}(\vec{r}) - \bar{n}_{I\alpha J\beta}) + \cdots]\phi_{J\beta}(\vec{r})\, d\vec{r}. \quad (17)$$

For the diagonal crystal-field terms ($I = J$ and $\alpha = \beta$) we can make the first-order term to go to zero, and minimize the second-order term, by expanding around $\bar{n}_{I\alpha,I\alpha}$ where

$$\bar{n}_{I\alpha,I\alpha} = \int \phi_{I\alpha}(\vec{r}) n^{(0)}(\vec{r}) \phi_{I\alpha}(\vec{r}) d\vec{r} = \sum_J n_{I\alpha J}, \quad (18)$$

and $n_{I\alpha J} = \int \phi_{I\alpha}(\vec{r}) n_J(\vec{r}) \phi_{I\alpha}(\vec{r})\, d\vec{r}$. Further, if we neglect the off-diagonal terms, we get

$$v_{\mathrm{xc},I\alpha I\beta}[n^{(0)}] = v_{\mathrm{xc}}\left(\sum_J n_{I\alpha J}\right)\delta_{\alpha\beta}. \quad (19)$$

This is the Sankey-Niklewski (SN) approximation [12]. Equation (19) treats many-center, as well as one- and two-center, contributions approximately. The SN correction requires only two-center integrals.

We can now get the SN many-center correction to the two-center crystal-field integrals by subtracting the two- and one-center contributions from Eq. (19):

$$\Delta v_{\mathrm{xc},I\alpha I\alpha} \approx v_{\mathrm{xc}}[\bar{n}_{I\alpha,I\alpha}] - v_{\mathrm{xc}}[\bar{n}_{I\alpha,I}] - \sum_{K\neq I}(v_{\mathrm{xc}}[\bar{n}_{I\alpha,I} + \bar{n}_{I\alpha,K}] - v_{\mathrm{xc}}[\bar{n}_{I\alpha,K}]). \quad (20)$$

We may also choose to only subtract the one-center terms, and remove the exact dimer contributions, effectively using the SN approximations for both two- and many-center integrals, in which case we end up with an expression very similar to the MCWEDA method [43].

F. Correcting hopping integrals

The easiest way to compare the hopping integrals computed using the two-center approximation with the exact results is to rotate all integrals so that their reference frame lies along the bond between the pair of atoms (the bond frame). When using the two-center approximation, these are conventionally written as $V_{ss\sigma}$, $V_{sp\sigma}$, $V_{pp\sigma}$, $V_{pp\pi}$, etc.

In order to transform between the bond frame and the simulation frame, we need the relevant rotation matrices for the orbitals: these are the ones used to determine the Slater-Koster tables. The matrices $D_{lm\tilde{m}}$ are given by the overlap between spherical harmonics in the bond frame ($|l\tilde{m}\rangle$ in Dirac notation) and in the simulation frame ($|lm\rangle$), hence,

$$|lm\rangle = \sum_{\tilde{m}} D_{lm\tilde{m}} |l\tilde{m}\rangle\,. \quad (21)$$

The matrix elements of the Hamiltonian H between orbitals in the simulation frame for a pair of atoms ($\langle l'm'n'|\, H\, |lmn\rangle$, where n and n' index the radial parts of the atomic orbitals) are related to the corresponding matrix elements in the bond frame ($\langle l'\tilde{m}'n'|\, H\, |l\tilde{m}n\rangle$) by

$$\langle l'm'n'|\, H\, |lmn\rangle = \sum_{\tilde{m},\tilde{m}'} D_{l'm'\tilde{m}'} D_{lm\tilde{m}} \langle l'\tilde{m}'n'|\, H\, |l\tilde{m}n\rangle\,. \quad (22)$$

Let us suppose we know the Hamiltonian matrix elements in the simulation frame by directly calculating them using a full calculation. We can now find the integrals in the bond reference frame using

$$\langle l'\tilde{m}'n'|\, H\, |l\tilde{m}n\rangle = \sum_{m,m'} E_{l'\tilde{m}'m'} E_{l\tilde{m}m} \langle l'm'n'|\, H\, |lmn\rangle\,, \quad (23)$$

where

$$E_{l\tilde{m}m} = D^{-1}_{lm\tilde{m}} = D^{T}_{lm\tilde{m}}. \quad (24)$$

Two-center integrals in the bond frame can be found from their values in the simulation frame exactly by using the Slater-Koster tables. This is not necessarily true for the many-center integrals, as the surrounding atoms can break the symmetry of the bond. For example, there is no guarantee that the bond-frame matrix elements $\langle p_x|\, H\, |p_x\rangle$ and $\langle p_y|\, H\, |p_y\rangle$ will be the same, even though these should both equal $V_{pp\pi}$, or that $\langle s|\, H\, |p_x\rangle$ or $\langle s|\, H\, |p_y\rangle$ will be zero. For each nonzero bond, an average value of the Slater-Koster projections was used in these cases. We will refer to this technique as the inverse Slater-Koster method.

G. Fitting tabulated integrals

The hopping integrals and the pair potential were fitted in this work. We represent the integrals using an analytical function adapted from Krishnapriyan's work [19]. The form used is a product of four terms:

$$f(r) = f_0 \zeta(r) N(r) T(r), \quad (25)$$

where f_0 is a constant corresponding to the value of $f(r)$ at a reference position r_0, $\zeta(r)$ is a radial decay function, $N(r)$ is a function that introduces nodes into the integrals, and $T(r)$ is a tail function that ensures that $f(r)$ decays smoothly to zero

at the cutoff value r_c. The forms for these functions are

$$\zeta(r) = \exp\left(\sum_{i=1}^{p} A_i (r - r_0)^i\right),$$
$$N(r) = \prod_{n=1}^{n_{\text{nodes}}} \frac{r - r_n}{r_0 - r_n},$$
$$T(r) = \exp\left(\frac{d}{r - r_c}\right), \tag{26}$$

where $d = 0.5a_0$, A_i are adjustable parameters, r_0 is a reference bond length, and r_n are the node positions. The number of nodes is taken from the initial tabulated (dimer) integrals. In all cases, the starting parameters (A_i and r_n) were taken from a fit to the initial tabulated integrals.

Hopping integrals are optimized to reproduce results from inverse-SK calculations on perfect crystals. Therefore, no reference data are obtained for bond lengths below $r_{\text{min}} \approx 5.3a_0$ for Zr and $r_{\text{min}} \approx 5.8a_0$ for Mg. To account for this we built the objective function from two parts: one measuring goodness of fit to the dimer integrals below r_{min}, and one measuring goodness of fit to the inverse-SK results. This was necessary to ensure reasonable values occurred below r_{min}. The goodness of fit to inverse-SK results was weighted by a factor of 100, in order to prioritize a good fit to these results. The numbers of adjustable parameters A_i vary between the hopping integrals, but are always between 3 and 5.

Pair potentials were fit to the equilibrium volume (V_0) and bulk modulus (B_0) of hcp and bcc structures from plane-wave DFT calculations (only the hcp structure was fit to for Zr). This was carried out using the same functional form as for fitting the hopping integrals, with four adjustable A_i parameters. The goodness of fit (GOF) for each quantity was calculated using a relative root-mean-square deviation function. For example, for V_0 we have

$$\text{GOF} = w \frac{\sqrt{\left(V_0 - V_0^{\text{ref}}\right)^2}}{V_0^{\text{ref}}}, \tag{27}$$

where w is a weighting factor, that was set to 10.0 for V_0 and 1.0 for B_0. The objective function is the sum of goodness-of-fit values for these properties.

The shortest bond length included in the fits (both hopping integrals and pair potential) was $5.8a_0$ for Mg and $5.3a_0$ for Zr. As a result, we found that, for Mg, an unphysically attractive potential occurred at short separations after the fitting process. To fix this, we made the pair potential highly repulsive at distances $r < 4.5a_0$ by fitting an exponential decay function to the dimer dissociation curve between $4.4a_0$ and $1.5a_0$ [the decay function was multiplied by $T(r)$ with $r_c = 4.5a_0$ to ensure this did not affect interactions beyond this point]. The objective function was set such that the energy at $4.4a_0$ separation matched the LCAO value, while the model interaction energy was greater than or equal to the LCAO value at all shorter distances (i.e., so the model is always at least as repulsive as LCAO at short distances).

H. Convention for naming approximations

We used a range of approximations in this work, and hence need to define a system to identify them. The summary of all the models used in this paper is shown on Fig. 2. LCAO is the label given to the method whereby we use the Harris-Foulkes functional up to first order and calculate all terms exactly. For other methods we approximate hopping integrals, crystal-field integrals, and the pair potential. Each method label is therefore made up of three components: hopping (H), crystal field (XT), and the pair potential (PP). These labels are followed by the approximations used for that contribution to the energy: for example, the method H_2b_XT_2b_PP_2b represents the case where we used tabulated dimer integrals (2b) with no correction to calculate all terms.

For hopping integrals, the two approximations are the dimer integrals (2b) or fitted integrals (fit). For crystal-field terms the approximations are the dimer integrals (2b), the dimer integrals plus the SN correction for many-center terms (2b_mbSN), or using the SN correction for two- and many-center terms (2bSN_mbSN). For the pair potential the possible options are dimer integrals (2b), dimer integrals plus the uniform density approximation (2b_uden), and a fitted pair potential (fit). The most complex method (in terms of naming) used in this paper is H_fit_XT_2b_mbSN_PP_fit_uden: this method uses fitted hopping integrals, dimer integrals plus the SN many-center correction for crystal-field terms and a fitted potential plus the uniform density approximation to represent the pair potential.

III. RESULTS

We now consider specific models we have generated, and assess their merits. We used a $20 \times 20 \times 12$ k-point grid for the hcp unit-cell calculations and equivalent for other structures. For the plane-wave calculations we used the CASTEP code with cutoffs of 450 eV for Zr and 500 eV for Mg [44]. We explicitly modeled semicore states in plane-wave calculations (but not LCAO calculations); plane-wave pseudopotentials with core charges of 10 and 12 were used for Mg and Zr, respectively. For LCAO calculations we used the PLATO TB code [45]. Further methodological details can be found in the ESI [46].

A. Basis-set selection

We first assess the effectiveness of the chosen basis sets for non-self-consistent calculations without any further approximations (see Table I). We wish to choose basis sets that best reproduce plane-wave structural properties. However, we also want r_c to be as small as possible: a smaller value of r_c means fewer integrals to compute and therefore greater computational efficiency, as well as fewer many-center interactions. We find that there is a minimum range that the basis set needs in order to be able to represent the electronic structure of hexagonal metals accurately, and which is transferable to other lattice structures. This transferability is important for the study of point defects, stacking faults, and dislocations.

Table I shows that the general effects of varying the radius of the confinement potential r_c are similar for both Mg and Zr. It was found that as r_c increases, so does the equilibrium lattice parameter of the resulting crystal structures.

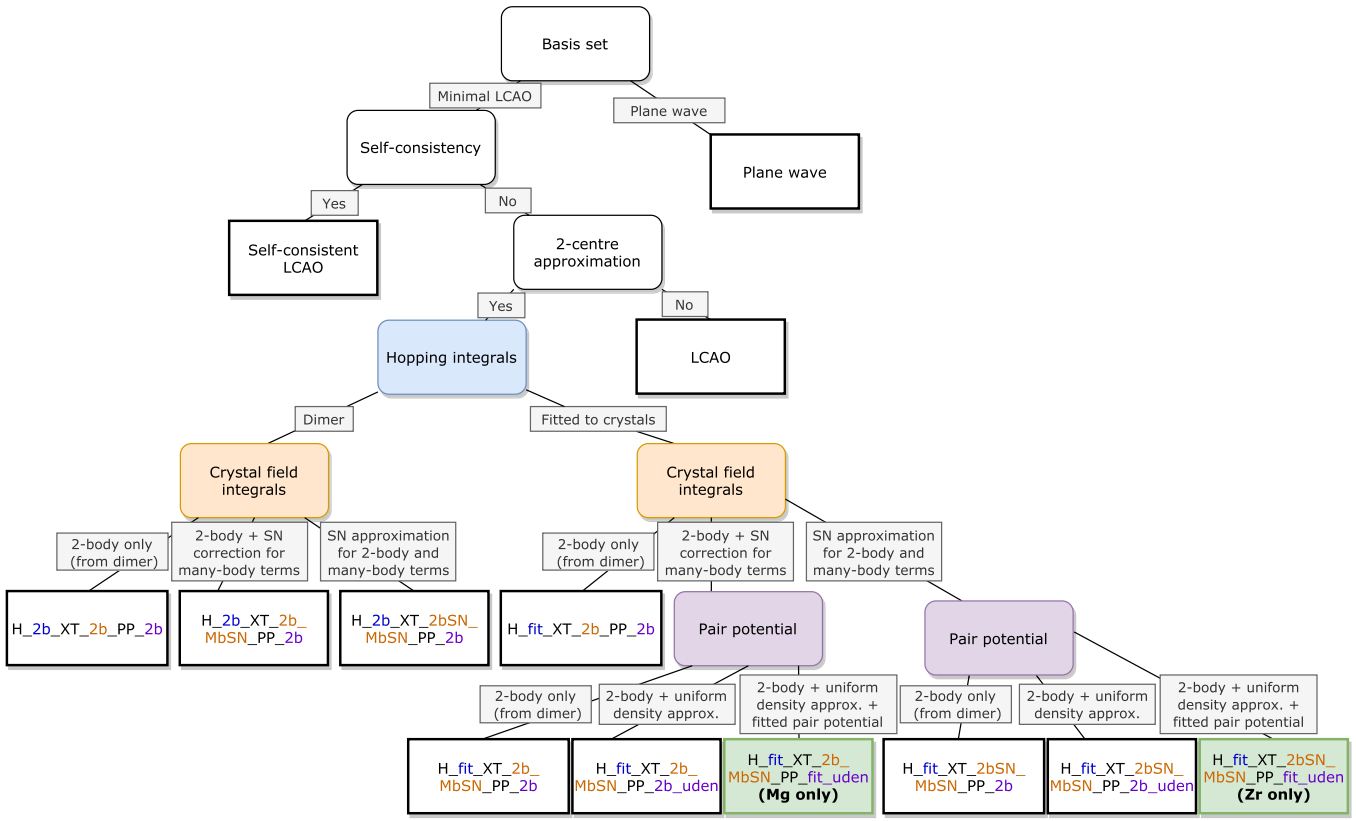

FIG. 2. A summary of the models compared in this paper. The final two-center tight-binding models for Zr and Mg are highlighted in green.

Furthermore, the energy ordering of the fcc and hcp structures is relatively independent of the confinement potential chosen (see ESI [46]). However, the bcc lattice becomes (relative to fcc and hcp) more stable as shorter-ranged orbitals were used.

The higher sensitivity of the structural energy difference between hcp and bcc in Zr can be understood from the electronic densities of states (Fig. 3): the bcc density of states shows only a small variation with the range of the basis set, while the close-packed structures show a much better agreement with the plane-wave basis set for basis sets with $r_0 \geqslant 6\,a_0$ than for shorter-ranged basis sets (see Fig. 3).

Basis sets with $r_c < 7.0a_0$ lead to poor structural properties for both Zr and Mg, and are therefore unsuitable. We chose to use basis sets with $r_c = 7.3a_0$ for both Mg and Zr since these give a good compromise between accuracy and speed. See Fig. 4 for the resulting energy against volume curves for the main structures.

The reduced sensitivity of the bcc structure to the basis-set range in Zr can be explained by considering the effect of the range of the $5p$ orbitals on E_1. The smaller the range of the confinement potential, the higher the on-site energy is of the empty atomic p orbitals, while the filled $5s$ and $4d$ orbitals are significantly less affected. However, when calculating E_1, the electronic structure states are a mix of these atomic orbitals. Therefore, raising the energy of the $4p$ orbitals will raise the energy of the electronic states containing them. In the bcc structures the majority of the filled electronic states have very little p orbital contribution compared to close-packed structures. This leads to E_1 for close-packed structures increasing more for a shorter-ranged basis set than for an

TABLE I. Dependence of physical properties on the confinement potential r_c used to generate the basis set for Mg and Zr. The value of r_0 appearing in the confinement potential was $r_c - 1.0a_0$ for Zr and $r_c - 1.5a_0$ for Mg.

	V_{eqm} (hcp) (a_0^3 per atom)		Bulk modulus (hcp) (GPa)		ΔE (bcc-hcp) (eV per atom)	
r_c (a_0)	Zr	Mg	Zr	Mg	Zr	Mg
6.0	139.4	144.0	145.4	62.5	−0.089	0.014
6.5	147.8	145.9	118.8	59.8	−0.020	0.014
7.0	153.7	153.2	100.1	45.9	0.021	0.025
7.3	156.9	155.9	95.4	41.8	0.038	0.029
7.5	155.6	157.4	90.2	39.8	0.032	0.030
8.0	157.7	160.3	84.0	38.7	0.068	0.031
Plane wave	157.8	154.4	90.7	36.0	0.082	0.029

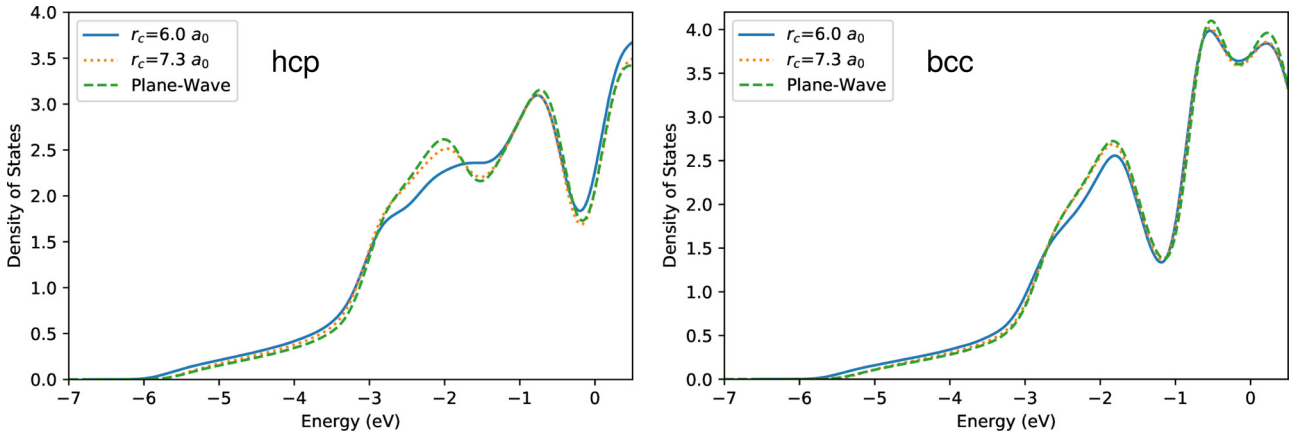

FIG. 3. The effect of the range of the confinement potential on the electronic density of states of hcp Zr. The longer-ranged LCAO orbitals offer a significantly better agreement with the plane-wave basis-set calculation.

equivalent bcc structure, and hence bcc becomes relatively more stable.

These results demonstrate that it is possible to get good structural and electronic properties for hcp metals using the Harris-Foulkes functional to first order combined with a single-ζ basis set. However, as we discuss below, the self-interstitial energies are found to be significantly too small for Zr.

B. Importance of self-consistency for defects

The way in which our basis sets were chosen (by comparison with a self-consistent plane-wave DFT calculation) means that the effects of self-consistency on equilibrium volumes are already implicitly accounted for. However, this self-consistency is not accounted for in defect energies, which are expected to be sensitive to self-consistency. We investigated this by carrying out LCAO calculations with full self-consistency using Kohn-Sham DFT with our small basis sets. The geometry for the relaxed defect calculations was found using plane-wave DFT and used in other methods without allowing for further relaxation.

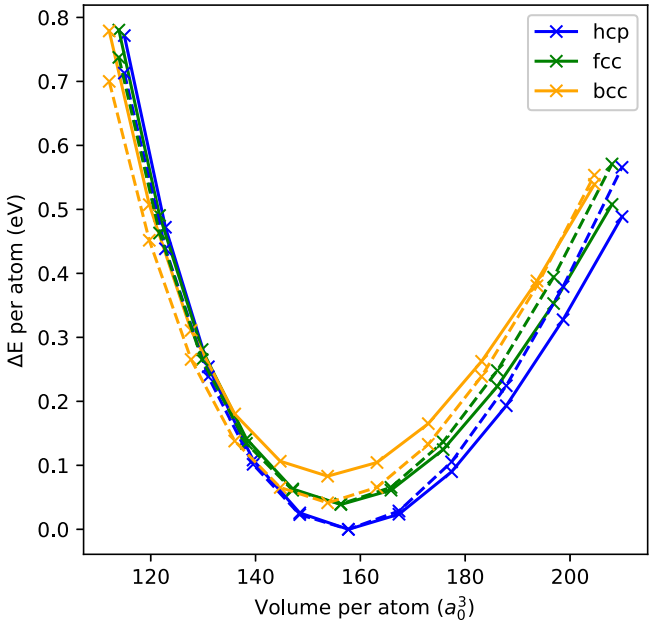

FIG. 4. A comparison of the energy versus volume curves for different lattice structures in Zr for LCAO with $r_{\text{cut}} = 7.3\,a_0$ (non-self-consistent calculation) and a plane-wave basis set (from CASTEP). Solid lines represent plane-wave (reference) data while dashed lines are LCAO data.

Self-consistency has only a minimal effect on defect energies for Mg (changes in energies no more than 0.03 eV) but has a more significant effect on Zr (see Table II). This dependence is reflected in the amount of charge transfer occurring in these structures; for Mg defects (both interstitial and vacancy) each Mg atom has an absolute Mulliken atomic charge of less than $0.02e$ while Zr atoms have charges up to $0.05e$ in the relaxed interstitial.

The differences between plane-wave and self-consistent LCAO calculations must result from the use of small basis sets. For both Mg and Zr the vacancy energies are overestimated (i.e., the vacancies are spuriously destabilized). This is what would be expected based on basis-set superposition errors (BSSE): the vacancy structure has fewer basis functions per volume than the perfect structure, which will likely spuriously destabilize it [47]. This effect may also contribute to the underestimation of the Zr interstitial energy: BSSE is expected to spuriously stabilize interstitials as there are extra orbitals available in the region around the interstitial. The implicit representation of semicore states using a pseudopotential may also contribute to the remaining errors in self-interstitial energies [48].

When studying defects in LCAO DFT, a much larger basis set would typically be used. The split-valence multiple-ζ basis set with explicitly included $4p$ states and a core correction used in SIESTA gives reasonably good agreement with plane-wave results for defects in Zr [49]. This basis set includes 13 localized functions, compared to the 9 used in this work [50].

We have tried splitting the basis set for Zr using the procedure implemented in SIESTA [37] with $5s$ and $4d$ orbitals being double-ζ. While this does lower all total energies calculated, the predicted lattice constants were consistently about 2% lower than the ones predicted by plane-wave code. Furthermore, the cohesive energies in compression were about

TABLE II. Selected structural and defect results for the methods tested. While plane-wave results are listed for reference, the accuracy of each approximation should be compared to LCAO as all other methods are approximations to this. A missing value means it could not be computed. The naming of the methods is explained in Sec. II H.

	Volume (a_0^3)		Unrelaxed vacancy energy (eV)		Relaxed octahedral self-interstitial energy (eV)	
Method	Zr	Mg	Zr	Mg	Zr	Mg
LCAO	156.9	155.9	2.56	1.08	1.97	2.61
H_2b_XT_2b_PP_2b			443.89	0.76	−240.64	−138.79
H_2b_XT_2b_MbSN_PP_2b			289.90	0.23	−122.64	−32.67
H_2b_XT_2bSN_MbSN_PP_2b			231.99	−0.01	−68.89	0.32
H_fit_XT_2b_PP_2b		225.1	31.27	−1.16	45.80	−1.17
H_fit_XT_2b_MbSN_PP_2b		224.5	0.97	−0.98	−1.58	−0.94
H_fit_XT_2bSN_MbSN_PP_2b		217.5	1.57	−1.14	−0.55	−0.54
H_fit_XT_2b_MbSN_PP_2b_uden		226.8	0.26	−1.24	−1.36	−1.25
H_fit_XT_2bSN_MbSN_PP_2b_uden	166.6	220.3	0.86	−1.40	−0.32	−0.84
H_fit_XT_2b_MbSN_PP_fit_uden		155.0		1.35		2.19
H_fit_XT_2bSN_MbSN_PP_fit_uden	157.0		1.34		1.74	
Self-consistent LCAO	155.2	158.7	2.67	1.06	2.71	2.58
Plane wave	157.9	154.5	2.13	0.81	3.03	2.49

0.5 eV lower than in plane-wave calculations, and the equilibrium cohesive energy of the bcc structure was lowered. The lower cohesive energies are probably a consequence of a combination of the LDA optimized pseudopotential used and the absence of the semicore states or a core correction. Since the predicted lattice constants were incorrect, further investigation using the split valence basis set was not pursued, and the single-ζ basis set was used.

C. Two-center TB

The simplest way to build an *ab initio* TB model is to take the integrals calculated from a dimer and use these in a purely two-center manner: we label this method H_2b_XT_2b_PP_2b. In this case an integral between two atoms is computed by finding the distance between those two atoms, looking up a value in the relevant integral table and applying Slater-Koster rules to account for rotations. This method means that all many-center effects are neglected; interactions between two atoms are assumed to be completely unaffected by any neighboring atoms.

Table II shows a selection of physical properties calculated with a range of methods. The H_2b_XT_2b_PP_2b method leads to a completely unphysical description of both Zr and Mg metallic systems; no minimum volume could be identified while self-interstitials are predicted to be very stable (e.g., the formation energy is −161.9 eV for Mg). These errors come primarily from the E_1 terms, as high-energy exact LCAO states are spuriously stabilized by the neglect of many-center effects. This can be seen visually in the density of states for the compressed hcp structures (see Fig. 5 for Zr and ESI [46] for Mg). For Zr the LCAO valence band states appear to have been shifted to ≈10 eV above the Fermi energy for the H_2b_XT_2b_PP_2b method. In the case of Mg, valence band states are present more than 20 eV below the Fermi level for the H_2b_XT_2b_PP_2b method, compared to about 8 eV for the exact LCAO method. The filled states correspond to states with large contribution from the p states, which then collapse to very low energies.

The failure of the H_2b_XT_2b_PP_2b method has two causes: errors in the Hamiltonian matrix elements and the small eigenvalues in the overlap matrix, which were calculated without approximation. For example, for the compressed Zr hcp structure used in Fig. 5, eigenvalues of the overlap matrix were as low as 0.005, which means the basis set produces states that are nearly linearly dependent. These small eigenvalues in the overlap matrix amplify errors in the Hamiltonian matrix elements when used to find eigenvalues. Similar problems have previously been discussed in the context of germanium semiconductors, suggesting this problem is not specific to hcp metals and will likely occur for other densely packed systems requiring a long-ranged basis set [51].

To gain greater accuracy than the H_2b_XT_2b_PP_2b method we need to either reduce errors in the Hamiltonian matrix elements or choose a basis with larger eigenvalues for the overlap matrix. Using shorter-ranged basis functions would lead to larger overlap eigenvalues, but we have already chosen the shortest-ranged basis set that gives reasonable results due to considerations of computational efficiency. We will therefore initially focus on corrections for E_1 terms, namely, the hopping and crystal-field integrals.

D. Hopping integrals

The two-center approximation for hopping integrals has been used widely, and with considerable success. Importantly, its accuracy can be improved over an initial DFTB estimate through numerical optimization [19], though it is not guaranteed that this is always possible. This procedure is only valid when, for a given bond length, the environmental effect on the bond is similar for all relevant structures. Here, we examine the magnitude and nature of the errors introduced by excluding the three- and higher-center integrals, but allowing for optimization of the two-center form.

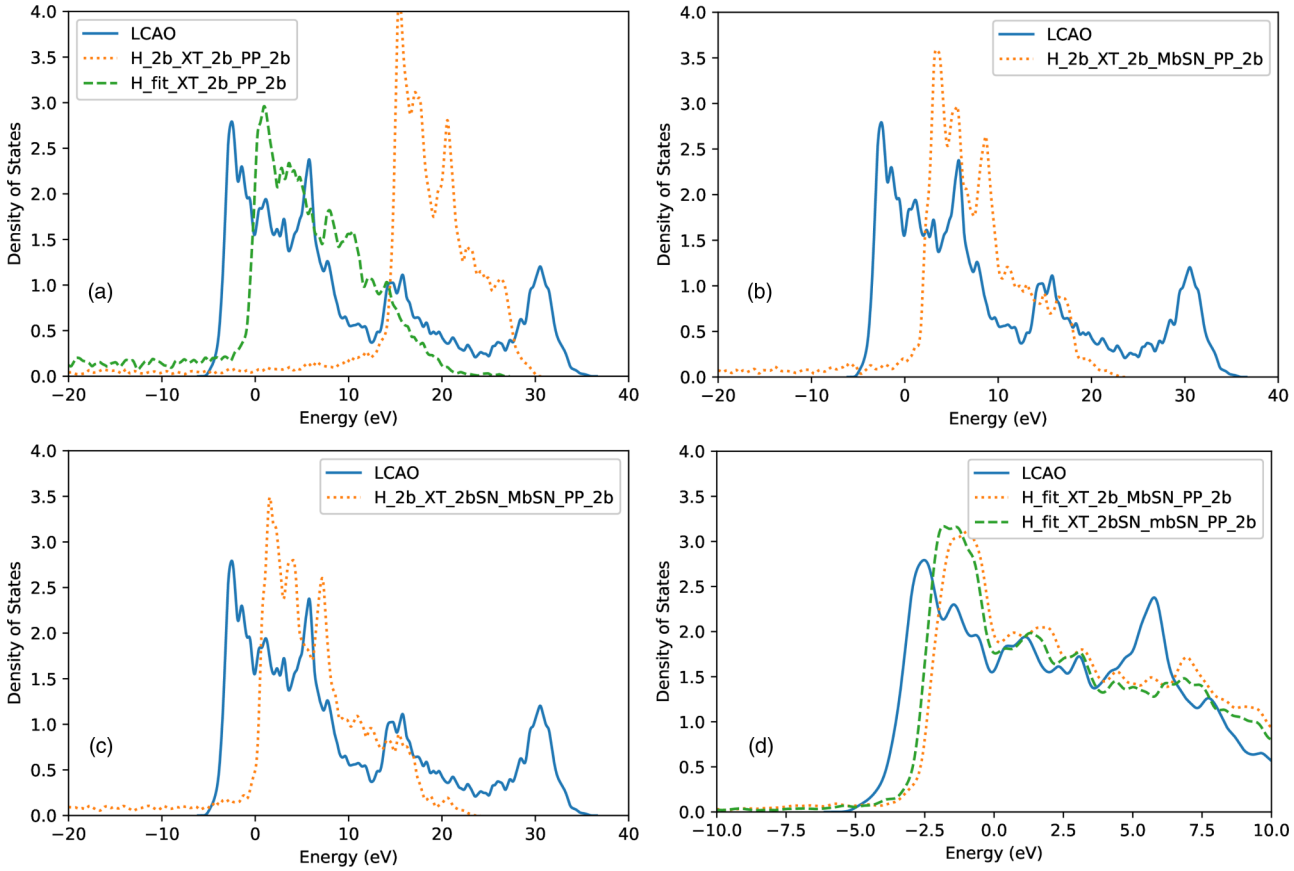

FIG. 5. Density of states for a compressed ($V \approx 115a_0^3$ per atom) hcp Zr structure using various methods. In each case, the Fermi level is at 0 eV. The subfigures show the effects of approximating and correcting the hopping integrals without correcting the crystal-field integrals (a), the two corrections for the crystal-field terms only (b), (c), and the corrections to both hopping and crystal-field integrals (d).

The inverse-SK method described above allows us to obtain the optimal two-center hopping integrals for a given structure. Comparing these with integrals from a dimer (referred to as dimer integrals below) allows us to better understand the errors in hopping integrals.

Figure 6 shows the inverse-SK hopping integrals for perfect Zr lattices alongside the dimer hopping integrals. The many-center interactions are strongest for the most extended orbitals (s and p for Zr) and for lattices in compression, and is reflected in the large differences between dimer and inverse-SK hopping integrals. This is as expected. An increased number of many-center interactions will be present if the lattice is compressed or if orbital ranges are increased; either case will lead to each bond effectively having more neighbors. In general, the magnitude of hopping integrals is underestimated by the dimer approximation. In particular, in the case of Zr p orbitals, this underestimation leads to some elements of the Hamiltonian matrices being too small. In combination with the underestimation of crystal-field terms (see below) and the small eigenvalues of the overlap matrix, this causes a very severe collapse of the band structure resulting in the spurious appearance and filling of very low-energy states.

In a periodic system, the eigenstates are Bloch states, and a Hamiltonian needs to be diagonalized at each k point. For a given $\vec{k}$, the Bloch transformed Hamiltonian matrix element is given by

$$\bar{H}_{I\alpha,J\beta}(\vec{k}) = \sum_L H_{I\alpha\vec{0},J\beta\vec{R}_L} e^{i\vec{k}\cdot\vec{R}_L}, \tag{28}$$

where $\vec{R}_L$ is the vector between the unit cells with atom I and a periodic image of atom J in cell L. At the gamma point, $\vec{k} = \vec{0}$, and the diagonal components are then given by

$$\bar{H}_{I\alpha,I\alpha}(\vec{0}) = \sum_L H_{I\alpha\vec{0},I\alpha\vec{R}_L}. \tag{29}$$

When $\vec{R}_L = \vec{0}$, this corresponds to the crystal-field terms combined with the atomic orbital energies, while the other terms in the sum are the different hopping integrals between an orbital on the atom I and its periodic images.

The propagation of errors in hopping integrals to calculated eigenvalues can be demonstrated most easily for single-atom unit cells. For the gamma point of an fcc lattice under 10% hydrostatic compressive strain (where all nondiagonal components are zero, making the eigenvalue calculation trivial), the difference between the components corresponding to p_x-p_x bonds in the two-center model and the many-center LCAO calculation is $-4.61 - 0.32 = -4.93$ eV. The difference between the corresponding on-site terms (and therefore crystal-field terms) is $2.57 - 3.93 = -1.36$ eV, which accounts for only 28% of the error in the Hamiltonian and therefore the corresponding eigenvalue; the remaining 72% is due to error

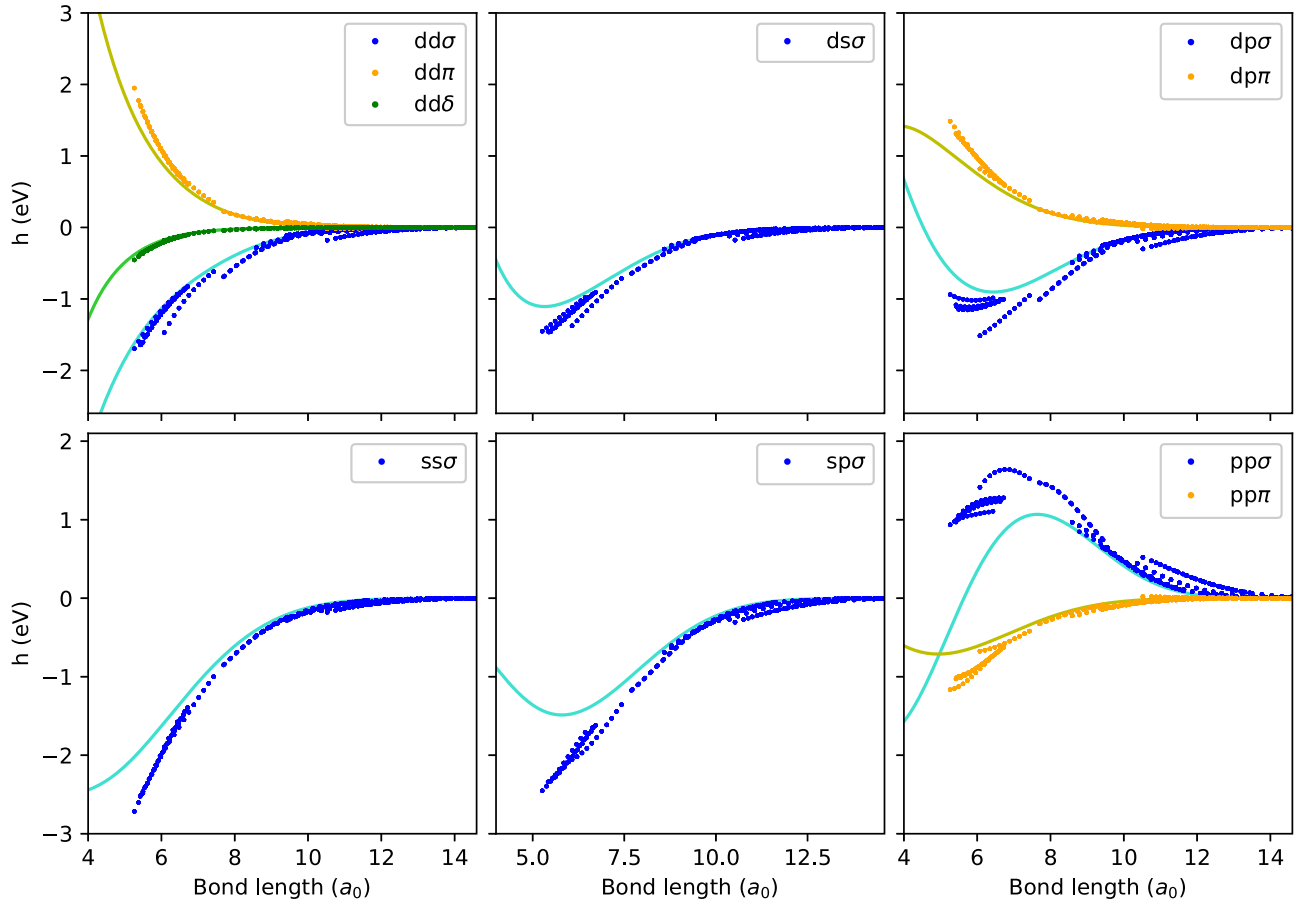

FIG. 6. The two-center hopping integrals for a dimer (solid lines) compared to the equivalent projections of these hopping integrals from a full many-center calculation in perfect Zr crystals (hcp, bcc, and fcc) with lattice constants varying from 90% to 110% of their equilibrium values.

in the hopping integrals. Because of the small value of the relevant overlap matrix terms, 0.0146, this causes the eigenvalue at this k point to be 337 eV lower in the two-center model compared to LCAO.

A method of correcting the hopping integrals, while keeping the two-center approximation, has been proposed previously, including a successful application to titanium band structure [28]: a curve is fit through the hopping integral projections from an LCAO DFT calculation, which corresponds to fitting to inverse-SK results in our case. This method relies on the hopping integrals being similar between all environments of interest since it still involves a single hopping integral for each separation. The spread in the inverse-SK results (i.e., how much the values vary for a single separation) is therefore an important factor in assessing the viability and limitations of this method.

For perfect periodic lattices, the spread in hopping integrals is the largest for σ bonds and for bonds between the most extended orbitals (see Fig. 6). A key problematic feature is the spread in the values for tails of these functions, i.e., for bond lengths larger than $10a_0$. The bonding integrals for lattices in compression in this region are much larger than for equivalent bond lengths for a lattice in tension. The individual contributions of these long bonds are relatively small compared to nearest neighbors and next-nearest neighbors, but there are a large number of neighbors at these distances, plus they make finding a smooth functional fit to the hopping integrals more difficult.

To find the origin of this spread in the hopping integrals, and then find a way to correct it, it is useful to look separately at the electrostatic plus kinetic energy contributions (including the nonlocal part of the pseudopotential, Fig. 7), and the exchange and correlation contributions (Fig. 8). Note that the kinetic energy term is exactly described by the two-center approximation. Figure 7 shows that the average shift of the electrostatic part of the hopping integrals is small compared to an equivalent dimer; however, the spread can be large compared to this shift. Some exact hopping integrals were larger in magnitude than the equivalent dimer and some smaller; the only general rule is the more compressed the lattice, the larger the deviation from the dimer value. The σ hopping integrals show the largest spread in the tails.

By contrast, the exchange and correlation contributions to the hopping integrals behave more predictably (see Fig. 8). Their absolute magnitude was larger than that of the corresponding kinetic plus electrostatic hopping integrals, so their contribution is far from negligible. However, the sign of the error was constant across the range of volumes and structures (e.g., the exchange and correlation inverse-SK integrals were always too negative for $ds\sigma$, while the electrostatic inverse-SK was either too positive or too negative). When adding the two contributions together, the spread from the electrostatic

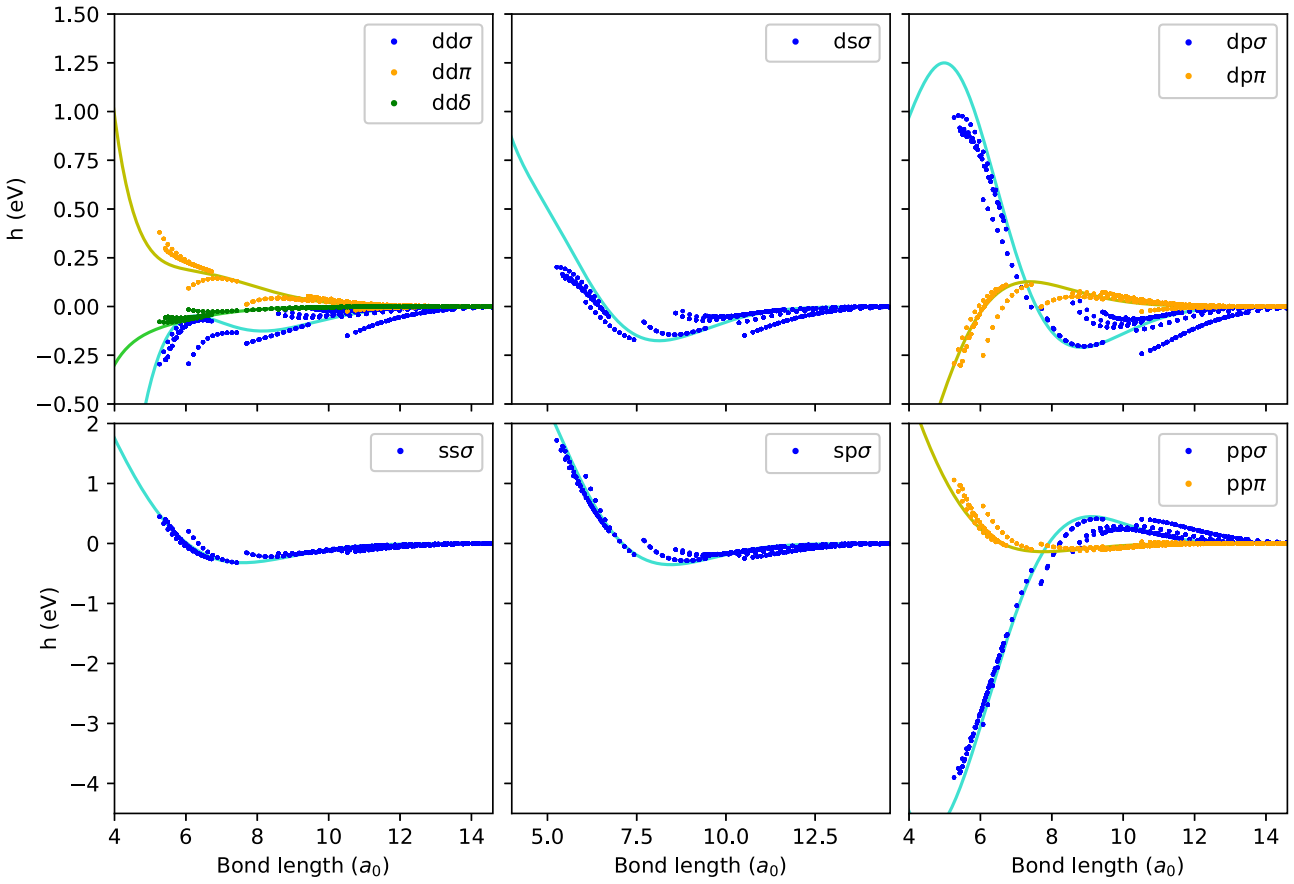

FIG. 7. The kinetic plus electrostatic part of the two-center hopping integrals for a dimer (solid lines) compared to the equivalent projections of these hopping integrals from a full many-center calculation in perfect Zr crystals (hcp, bcc, and fcc) with lattice constants varying from 90% to 110% of their equilibrium values.

contributions dominates the tails, while the overall increase in magnitude from exchange and correlation dominates the shorter bonds. The spread for shorter bonds is a result of a relatively equal combination of both contributions, which can sometimes partially cancel out.

Table II shows how calculated properties are affected by fitting to inverse-SK hopping integrals (details of the fit process are given in Sec. II G). The H_fit_XT_2b_PP_2b method provides a direct comparison with the simplest *ab initio* TB scheme. Fitting to inverse-SK results led to a marked improvement in calculated properties; for Zr the absolute vacancy and interstitial energies decrease by an order of magnitude while for Mg a minimum volume is obtained and the (spuriously negative) self-interstitial energy has increased by two orders of magnitude, though it is still spuriously stable. This improvement in physical properties is reflected in the more accurate electronic structure, as shown by the density of states in Fig. 5 and ESI [46]. States which were previously 10 eV above the Fermi energy are shifted to the top of the valence band after fitting the hopping integrals, leading to a much improved (though still relatively poor) agreement with LCAO results. Mulliken population analysis shows a reduction in p-orbital population from $2.71e$ (H_2b_XT_2b_PP_2b) to $1.77e$ (H_fit_XT_2b_PP_2b) after fitting hopping integrals (for a two-atom hcp unit cell). This is consistent with the Zr p inverse-SK hopping integrals showing large deviations from the dimer integrals.

Despite the large improvements in results after fitting the hopping integrals, this was insufficient to get a stable model for either Mg or Zr. One limitation of our method is that our functional forms were designed to have very small values in the tails, which is not necessarily true for the inverse-SK integrals. While we could use more flexible forms, this comes with the risk of overfitting. Another limitation is that the spread in inverse-SK hopping integrals means that the fitted integrals are a compromise between those that would be ideal for each of the individual structures. This is especially noticeable in the $pp\sigma$ hopping integrals for both Mg and Zr between $6a_0$ and $8a_0$, where the inverse-SK results are clearly discontinuous (Fig. 6). The discontinuous nature is partly due to the discontinuity between first and second neighbors in bcc structures, which is a well-known effect caused by the very different environments around these two bonds [52,53]. If interstitials were included, this discontinuity would be even more severe. Figure 9 shows inverse-SK results for self-interstitials alongside results from perfect crystals and the dimer hopping integrals. For bond lengths of $6a_0$ and above, there are significant differences in the results from perfect crystals and self-interstitial structures; in some cases even the sign of the correction (relative to the dimer integrals) is different between the two data sets.

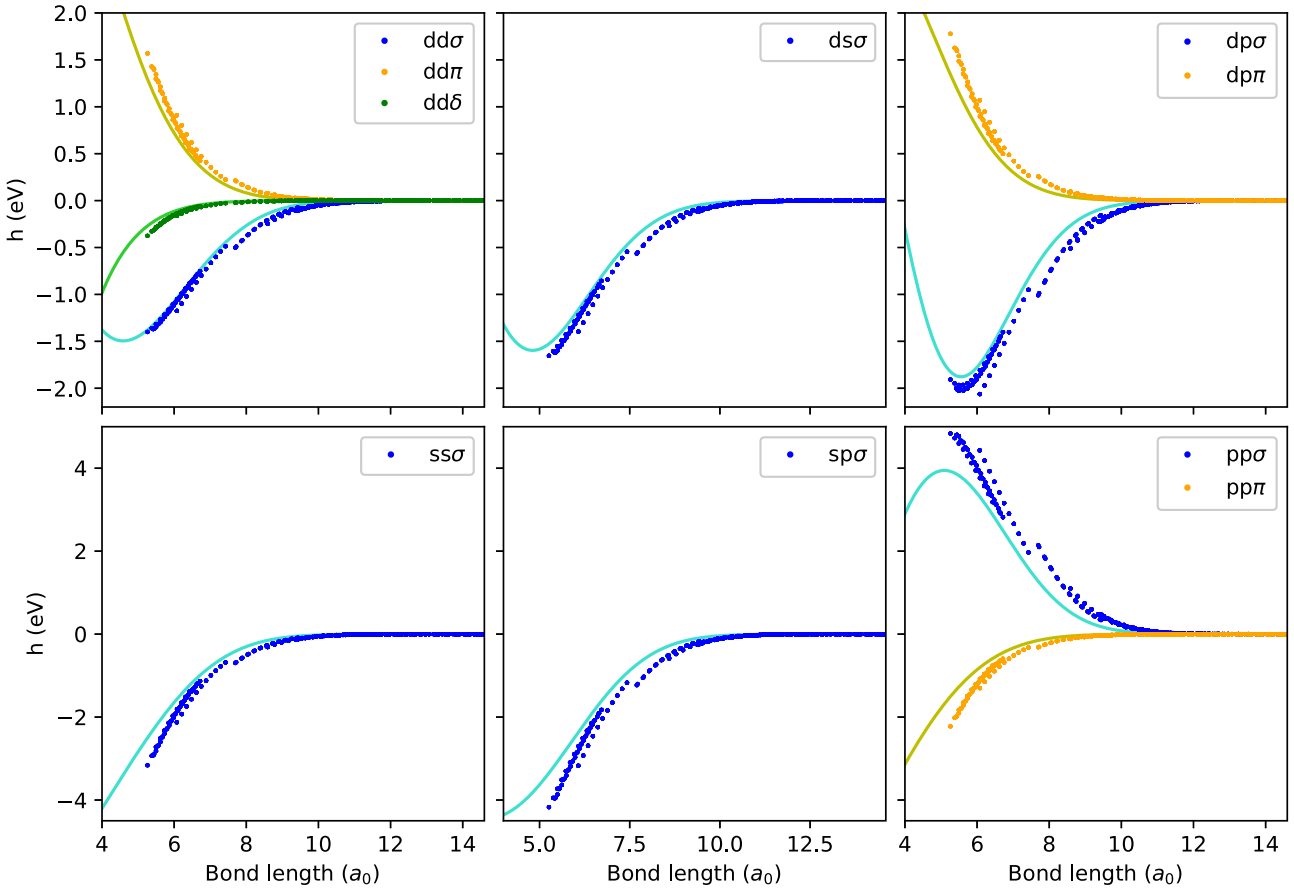

FIG. 8. The exchange and correlation contribution to the two-center hopping integrals for a dimer (solid lines) compared to the equivalent contribution to projections of these hopping integrals from a full many-center calculation in perfect Zr crystals (hcp, bcc, and fcc) with lattice constants varying from 90% to 110% of their equilibrium values.

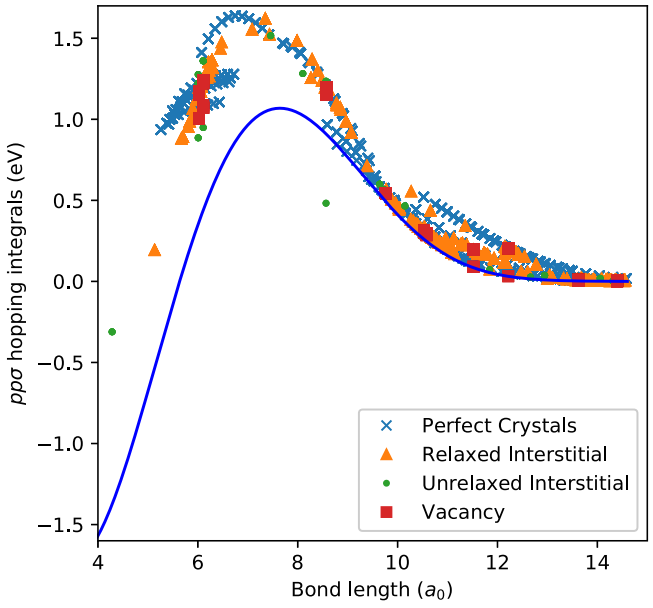

FIG. 9. The projected $pp\sigma$ hopping integrals from a full LCAO calculation (markers) compared to the two-center dimer approximation (solid line) for various structures of Zr. Perfect crystals include hcp, bcc, and fcc with lattice constants varying from 90% to 110% of their equilibrium values.

E. Crystal-field integrals

The on-site terms in the Hamiltonian have two parts: a contribution from the atom on which the orbitals are centered (the atomic term) and the contributions from the neighboring atoms (the crystal-field terms). The electrostatic contributions to the crystal field are strictly pairwise, while the exchange and correlation contribution includes many-center contributions. Our starting point for the discussion of the exchange and correlation contribution to the crystal field is the two-center approximation whereby the only error is from the missing many-center exchange and correlation contributions.

Consider the results for Zr shown in Fig. 10. The two-center approximation for crystal-field integrals (solid lines in Fig. 10) leads to underestimation of the on-site energies, which gets more severe as volume decreases. This effect is largest for the most extended orbitals (s and p), which is unsurprising as longer-ranged orbitals will participate in more many-center interactions for a given volume. The orbital dependence of these errors causes a relative stabilization of states containing s and p orbital contributions, which contributes to the significant differences in the density of states between LCAO and H_2b_XT_2b_PP_2b22. The decrease in on-site energies, with decreasing volumes, also provides a spurious stabilization to low-volume structures, which contributes to the instability of many of the tested tight-binding models (Table II).

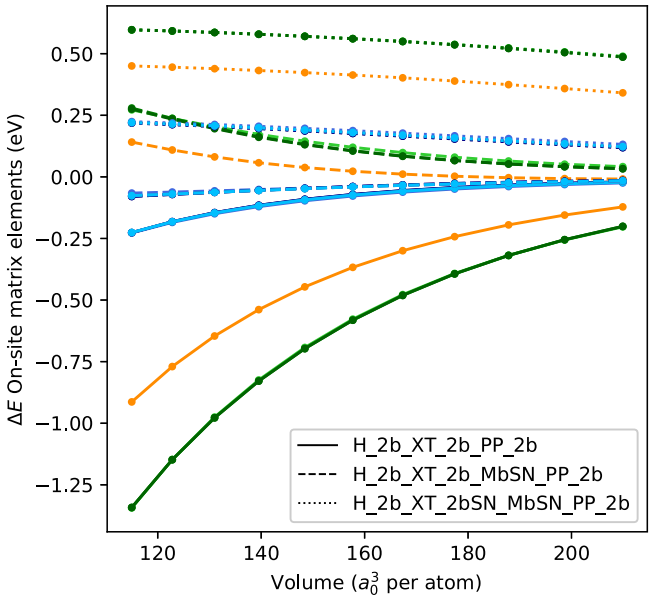

FIG. 10. Error in diagonal on-site matrix elements for strained hcp Zr (model minus LCAO) for various crystal-field approximations. Different colors correspond to different orbitals: *s* orbitals are orange, *p* orbitals are green, and *d* orbitals are blue. The line types correspond to different model approximations, as indicated in the legend in the figure.

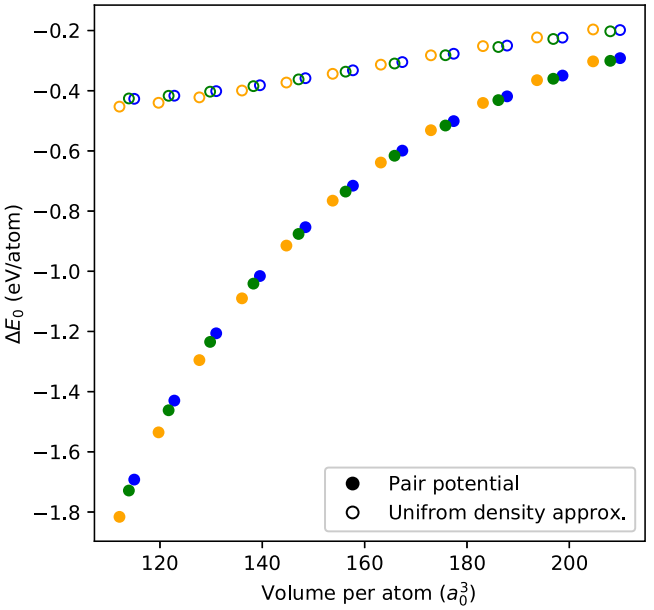

FIG. 11. The error in E_0 (model minus LCAO), for hcp (blue), fcc (green), and bcc (orange) Zr crystals.

The direct effects of the crystal-field approximations are best shown by comparison of the H_2b_XT_2b_mbSN_PP_2b (dashed lines) and H_2b_XT_2bSN_mbSN_PP_2b (dotted lines) methods with the uncorrected H_2b_XT_2b_PP_2b method (solid lines) in Fig. 10. Both correction schemes greatly reduce the volume dependence of on-site errors and, consequently, compression of perfect structures does not lead to spurious stabilization of the diffuse orbitals when using these corrections for the strained perfect crystals.

For Zr, using the SN correction for both two-center and many-center terms appears to lead to the best results. This is reflected in the reduced volume dependence seen in Fig. 10, and the improved density of states for compressed hcp relative to LCAO shown in Fig. 5. The improved DoS for H_2b_XT_2bSN_MbSN over H_2b_XT_2b_MbSN is likely due to the former correction overestimating on-site matrix elements, leading to a spurious destabilization of states, which cancels out with the spurious stabilization due to the hopping integrals. Thus, the SN correction will be used for both two-center and many-center crystal-field effects for Zr henceforth.

The corresponding results for Mg can be found in the ESI [46]. For Mg, the volume dependence of both crystal-field corrections was similar. However, in this case the H_2b_XT_2b_MbSN method led to smaller absolute errors in on-site energies and was therefore chosen in the final model.

In summary, we have shown that treating crystal-field terms using a two-center approximation leads to strongly volume-dependent errors (as smaller volumes mean more neglected many-center interactions). However, these errors can be largely mitigated using the SN correction. Applying this correction can be expected to lead to a more accurate TB model at no significant extra computational cost.

F. Corrections to the pair potential

As noted above, the two-center approximation for E_0 only introduces an error in the many-center exchange and correlation contributions. For both perfect Zr and Mg crystals E_0 is consistently underestimated (too negative) when the pair potential from a dimer is used: for example, for Zr this error is as large as 1.8 eV/atom under a 10% compression (see Fig. 11). Since the errors are largest in compression, this would result in all lattice parameters being too small, if it was the only source of error.

Remarkably, we find the error from the pair approximation is mostly structure independent, and mainly varies with the volume occupied by each atom (see Fig. 11). There is a slight structural dependence for Mg, with bcc being destabilized by the dimer pair potential, but this still only leads to an increase of less than 0.01 eV/atom for the relative equilibrium energy. We note that a pair-potential expression for energy cannot differentiate between an fcc lattice and a hcp lattice with an ideal c/a ratio. The energy difference between these two close-packed structures is therefore primarily determined by the higher-order terms. We note that E_1 is crucially needed to stabilize hcp.

Having established that a pair potential is insufficient, we now seek a correction. Figure 11 shows the effect of adding the nearly uniform density approximation correction (described in Sec. II D) for Zr (see ESI [46] for Mg). This correction reduces the error in compression to below 0.5 eV/atom (see Fig. 11) for Zr. Furthermore, this correction shows a far weaker volume dependence than using a pair potential alone. Another option for reducing the error in E_0 would be to fit a pair potential, as is commonly done in TB models. However, our uniform density correction is expected to be more transferable as it is a purely *ab initio* correction and is environmentally dependent. This environmental dependence does not add any significant computational overhead since

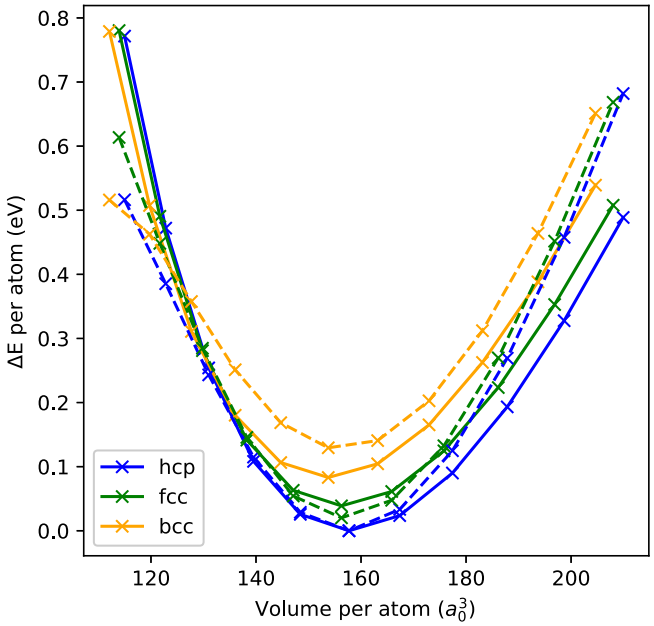

FIG. 12. Calculated energy against volume curves using plane-wave DFT (solid lines) compared to those calculated using our TB model for Zr (dashed lines).

the correction still only relies on tabulated two-center terms. Furthermore, it is possible to combine this correction with a fitted pair potential; this may provide greater transferability than a standard fitted pair potential without losing accuracy on the systems of most interest, and is the approach we take below.

G. Final TB models

Combining the most accurate individual approximations from above leads us to the tight-binding models presented in this paper. The model consists of using fitted hopping integrals, the SN correction for crystal-field terms, and the uniform density approximation to correct E_0. However, all these approximations together were still insufficient to produce a model as accurate as we would like, i.e., a reasonable approximation to LCAO DFT. Therefore, we also fit a pair potential to the models, and the resulting methods are labeled H_fit_XT_2b_mbSN_PP_fit_uden for Mg and H_fit_XT_2bSN_mbSN_PP_fit_uden for Zr. The objective function was a combination of hcp (also bcc for Mg) V_0 and B_0 values, as described in Sec. II G.

Figure 12 and ESI [46] show that the models with fitted pair potentials show good agreement for the energy against volume curves; V_0 for the hcp structure is given in Table II. This is unsurprising due to relevant terms being in the objective function for fitting the pair potential, and these structures being used to fit the hopping integrals. However, it is worth noting that the fcc structural parameters were not included in the pair-potential fit, and that none of the differences in energies between structures were fit (bcc structural parameters were also not included for Zr).

Both Mg and Zr models show reasonable agreement with plane-wave results for the unrelaxed elastic constants (see the ESI [46]); the average relative root-mean-square deviation ($\frac{\sqrt{(c_{\mathrm{TB}}-c_{\mathrm{ref}})^2}}{c_{\mathrm{ref}}}$) was 0.29 and 0.25 for Mg and Zr models, respectively. For comparison, previous tight-binding models for Mg and Zr led to values of 0.38 and 0.23, respectively (for relaxed elastic constants compared to experiment) [25,54].

For the unrelaxed hcp(0001) surface energy the Zr model leads to good agreement with both LCAO and plane-wave results (0.0275 eV a_0^{-2} for the final model compared to 0.0296 eVa_0^{-2} for plane-wave results, see the ESI [46]). Note that this good agreement likely stems partly from error cancellation between missing self-consistency effects and effects of our limited basis; this is shown by the LCAO method leading to better agreement with the plane-wave method than the self-consistent LCAO method. In contrast to Zr, the Mg model significantly overestimates the surface energy compared to plane-wave and LCAO methods (0.0246 eV a_0^{-2} for the final tight-binding model compared to 0.0098 eV a_0^{-2} for plane-wave results).

Errors in vacancy energies are substantial (slightly over 1 eV for Zr), but similar to many previous TB models [55,56]. The relaxed self-interstitial energies show good agreement with the LCAO results and also the plane-wave result for Mg. However, the plane-wave Zr self-interstitial energy is substantially underestimated as a result of our models lacking an approximation (either implicit or explicit) for self-consistency. Note that neither the vacancy nor self-interstitial structures were fit at any point, and their formation energies therefore represent true tests of the transferability of the models.

A key step toward obtaining accurate structural properties in these TB models was the fitting of the pair potential. The fitted pair potential (ESI [46]) is more attractive than the originally tabulated pair potential in the region around $6a_0$. This distance is that of first-neighbor interactions in the crystal; therefore, E_1 appears to have underestimated the interaction strength in this range. This is also the range where the inverse-SK hopping integrals have largest spread of values in the perfect crystal structures, and hence where the fit is least good. This underestimation of first-neighbor interactions can be used to rationalize the failures of models using fitted hopping integrals but not a fitted pair potential. The overestimation of V_0 is expected if first-neighbor interactions are spuriously repulsive. The vacancy structure contains fewer first-neighbor interactions per atom than the perfect crystal, and is therefore stabilized (relative to the perfect crystal) when these interactions are too repulsive (meaning a spuriously stabilized vacancy energy). Similarly, the relaxed interstitial structure has fewer metal-metal interactions at about $6a_0$ compared to the perfect structure, hence, the overstabilization before fitting the pair potential.

IV. DISCUSSION

Our results in this work first demonstrate the importance which many-center terms have on the electronic and structural properties of hcp metals. Without accounting for these terms, the models produced are inherently unstable, as the band structure tends to acquire states with large negative energies when the crystal is compressed. However, we produced two-center TB models that accurately reproduce struc-

tural and electronic properties for near-equilibrium structures. Nonetheless, it is important to be aware of the limitations of these models.

As already noted, the models are not expected to work well under high levels of compression. This is partly because we only fit hopping integrals to near-equilibrium structures and partly because we had to fit an unphysically repulsive potential for Mg-Mg separations smaller than $4.5a_0$ in order to ensure the model's stability (see Sec. II G). Even with this restriction, we found that an unrelaxed octahedral self-interstitial in Mg was spuriously stabilized (it had a formation energy of -51 eV). The situation for Zr is similar, with an unrelaxed octahedral interstitial having a formation energy of -28 eV. While the activation energies of these structures will likely mean they wont be accessible in most simulations, this coupled with the very repulsive potential below $4.5a_0$ for Mg and the lack of a correction for self-consistency for Zr means the models would not be appropriate for investigating self-interstitial formation, and that care may be needed when using them in general. We aim to address these concerns in future work.

Overcoming the deficiencies of the models presented here will require a different approach to the many-center contributions to the hopping terms. In particular, for studying defects, these integrals need to have an explicit environmental dependence: the optimal hopping integrals (from inverse-SK results) show significant differences between perfect structures and those with defects. There are (at least) two possible routes to achieve this.

Empirically fitting hopping integrals to a screening function is a method which has been used successfully for a range of systems including Cu, C, Mo, and Ge [57–61]. Particularly relevant is the work on Ge where reasonable defect energies were obtained despite only fitting to perfect crystal structures [58]: e.g., the vacancy formation energy was 2.82 eV compared to 2.42 eV from DFT. Despite the success of this method, it has drawbacks. First, calculation of screening functions (different ones for each hopping integral) means a less computationally efficient method. Second, a large number of parameters are required that lead to the risk of overfitting and makes the fitting process itself difficult, especially if fitting to bulk-phase properties since all parameters need to be fit simultaneously. These difficulties in fitting were overcome in work by Goldman, whereby the screening function parameters were fit to reproduce the hopping integrals for a series of trimer structures [61]. This allows each hopping integral to be fit independently of the others and transferability is expected to be high. In our case, this would correspond to running inverse-SK calculations on a series of trimers and fitting those. However, in the work of Goldman it was still necessary to manually tune (it was not specified how or to what extent) the d-d integrals to reproduce bulk properties.

Previously used corrections involved multiplying the calculated screening function by an environmentally independent (e.g., our dimer integral values) hopping integral. This is problematic for our systems where the dimer hopping integrals have multiple nodes in them at values where the many-center hopping corrections are significant (e.g., the $pp\sigma$ integrals for Zr). It is unclear how to apply a screening correction in this case.

An *ab initio* approach could also be used, such as is employed in the FIREBALL code, to provide environmental dependence to hopping integrals [43,62]. In this case, the neutral atom contributions to hopping integrals are calculated exactly, while the exchange-correlation contributions are approximated using a framework based on a Taylor series expansion around reference densities (i.e., similar to the SN and uniform-density approximations used in this work). Compared to the use of screening functions the lack of fitting required in this method means it should be easier to apply, especially when adding elements to a model, and is expected to have greater transferability. However, this method has the major disadvantage of requiring calculation of three-center integrals (though in FIREBALL this is achieved with tables of only two dimensions), and will therefore be significantly slower than the approach in this paper.

V. CONCLUSIONS

The process of building a systematic TB model for hexagonal metals starting from the DFTB approximation was introduced in this paper, with a focus on the errors introduced and possible corrections. While the method could be equally applied to other materials, the problems discussed are specific to close-packed materials with highly delocalized orbitals. In fact, the authors believe that for more suitable materials (notably ones with an open structure), the method presented could be used directly.

In the materials considered here (Mg and Zr), it has been shown that fairly long-ranged orbitals are needed in order to reproduce the electronic structure accurately and obtain the correct lattice constants and structural stability. This leads to important contributions from many-center terms in the hopping, crystal-field, and pair-potential integrals tabulated using DFTB. Without any corrections, the inaccuracies in these integrals lead to unphysically low electronic energy states associated with the most extended orbitals. Systematic corrections to the exchange and correlation parts of the crystal-field and pair-potential terms were introduced in the form of an embedding function. Corrections for both these terms significantly improved both Zr and Mg models for very little additional computational overhead. All of the corrections can be tabulated in terms of two-center terms.

The two-center approximation for hopping integrals introduces the largest errors and needs to be structure dependent. We have shown that while it is relatively easy to correct for most of the many-center errors by using a list of selected structures, even two bonds within the same structure of the same length can have very different hopping integrals, as is the case for an unrelaxed vacancy or interstitial, making it incompatible with the two-center approximation. To a lesser extent, the strained and compressed structures can also be incompatible, as well as an equilibrium structure compared to ones with relaxed point defects. Bonds will be strongly affected by atoms near them, and correcting for this environmental dependence in a computationally efficient way has not been fully successful in this work.

Another limiting factor in the modeling of point defects in Zr is the lack of semicore states. Self-consistency is also necessary for the calculation of the defect formation energies

as the charge transfer between the different atoms is significant (electrons are highly delocalized). While a larger basis set is not in the spirit of TB, it is not difficult to add following the same method as described above. Self-consistent TB is also a fairly standard technique described extensively in the literature [63].

ACKNOWLEDGMENTS

We thank A. Sutton for many important conversations on TB models. This work has in part been performed within the framework of the international MUZIC (Mechanistic Understanding of Zirconium Corrosion) program. The authors gratefully acknowledge the industrial support from EDF, EPRI, Naval Nuclear Laboratory, Rolls-Royce, Westinghouse, and Wood. J.S. gratefully acknowledges support through a studentship in the Centre for Doctoral Training on the Theory and Simulation of Materials at Imperial College London, funded by EPSRC under Grant No. EP/L015579/1, and by Rolls-Royce. R.M.F. gratefully acknowledges funding from EPSRC under Grant No. EP/R005419/1. We acknowledge support from the Thomas Young Centre under Grant No. TYC-101.

[1] W. Kohn and L. J. Sham, Phys. Rev. **140**, A1133 (1965).
[2] M. S. Daw and M. I. Baskes, Phys. Rev. B **29**, 6443 (1984).
[3] W. Kohn, A. D. Becke, and R. G. Parr, J. Phys. Chem. **100**, 12974 (1996).
[4] M. J. Gillan, D. R. Bowler, A. S. Torralba, and T. Miyazaki, Comput. Phys. Commun. **177**, 14 (2007).
[5] C.-K. Skylaris, P. D. Haynes, A. A. Mostofi, and M. C. Payne, J. Chem. Phys. **122**, 084119 (2005).
[6] B. Christiaen, C. Domain, L. Thuinet, A. Ambard, and A. Legris, Acta Mater. **179**, 93 (2019).
[7] M. I. Mendelev and G. J. Ackland, Philos. Mag. Lett. **87**, 349 (2007).
[8] M. J. Noordhoek, T. Liang, Z. Lu, T.-R. Shan, S. B. Sinnott, and S. R. Phillpot, J. Nucl. Mater. **441**, 274 (2013).
[9] J. C. Slater and G. F. Koster, Phys. Rev. **94**, 1498 (1954).
[10] D. J. Chadi, Phys. Rev. B **19**, 2074 (1979).
[11] A. P. Sutton, M. W. Finnis, D. G. Pettifor, and Y. Ohta, J. Phys. C: Solid State Phys. **21**, 35 (1988).
[12] O. F. Sankey and D. J. Niklewski, Phys. Rev. B **40**, 3979 (1989).
[13] W. M. C. Foulkes and R. Haydock, Phys. Rev. B **39**, 12520 (1989).
[14] A. P. Horsfield, Phys. Rev. B **56**, 6594 (1997).
[15] C. Goringe, D. Bowler, and E. Hernandez, Rep. Prog. Phys. **60**, 1447 (1997).
[16] T. Frauenheim, G. Seifert, M. Elsterner, Z. Hajnal, G. Jungnickel, D. Porezag, S. Suhai, and R. Scholz, Phys. Status Solidi B **217**, 41 (2000).
[17] A. Horsfield, Phys. Status Solidi B **249**, 231 (2012).
[18] L. Goodwin, A. J. Skinner, and D. G. Pettifor, Europhys. Lett. **9**, 701 (1989).
[19] A. Krishnapriyan, P. Yang, A. Niklasson, and M. Cawkwell, J. Chem. Theory Comput. **13**, 6191 (2017).
[20] M. S. Tang, C. Z. Wang, C. T. Chan, and K. M. Ho, Phys. Rev. B **53**, 979 (1996).
[21] C. H. Xu, C. Z. Wang, C. T. Chan, and K. M. Ho, J. Phys.: Condens. Matter **4**, 6047 (1992).
[22] D. Papaconstantopoulos and M. Mehl, J. Phys.: Condens. Matter **15**, R413 (2003).
[23] G. K. H. Madsen, E. J. McEniry, and R. Drautz, Phys. Rev. B **83**, 184119 (2011).
[24] T. Sheppard, A. Lozovoi, D. Pashov, J. Kohanoff, and A. Paxton, J. Chem. Phys. **141**, 044503 (2014).
[25] I. Schnell, M. D. Jones, S. P. Rudin, and R. C. Albers, Phys. Rev. B **74**, 054104 (2006).
[26] A. Dufresne, F. Ribeiro, and G. Tréglia, J. Phys.: Condens. Matter **27**, 336301 (2015).
[27] E. J. McEniry, G. K. H. Madsen, J. F. Drain, and R. Drautz, J. Phys.: Condens. Matter **23**, 276004 (2011).
[28] A. Urban, M. Reese, M. Mrovec, C. Elsässer, and B. Meyer, Phys. Rev. B **84**, 155119 (2011).
[29] N. Hatcher, G. K. H. Madsen, and R. Drautz, Phys. Rev. B **86**, 155115 (2012).
[30] C.-Z. Wang, W.-C. Lu, Y.-X. Yao, J. Li, S. Yip, and K.-M. Ho, Sci. Model. Simul. SMNS **15**, 81 (2008).
[31] M. Christensen, W. Wolf, C. Freeman, E. Wimmer, R. Adamson, L. Hallstadius, P. Cantonwine, and E. Mader, J. Nucl. Mater. **445**, 241 (2014).
[32] M. Christensen, W. Wolf, C. Freeman, E. Wimmer, R. Adamson, L. Hallstadius, P. Cantonwine, and E. Mader, J. Nucl. Mater. **460**, 82 (2015).
[33] S. Thomas, N. V. Medhekar, G. S. Frankel, and N. Birbilis, Curr. Opin. Solid State Mater. Sci. **19**, 85 (2015).
[34] J. Harris, Phys. Rev. B **31**, 1770 (1985).
[35] H. Eschrig and I. Bergert, Phys. Status Solidi B **90**, 621 (1978).
[36] S. D. Kenny, A. P. Horsfield, and H. Fujitani, Phys. Rev. B **62**, 4899 (2000).
[37] J. M. Soler, E. Artacho, J. D. Gale, A. García, J. Junquera, P. Ordejón, and D. Sánchez-Portal, J. Phys.: Condens. Matter **14**, 2745 (2002).
[38] V. Blum, R. Gehrke, F. Hanke, P. Havu, V. Havu, X. Ren, K. Reuter, and M. Scheffler, Comput. Phys. Commun. **180**, 2175 (2009).
[39] S. Goedecker, M. Teter, and J. Hutter, Phys. Rev. B **54**, 1703 (1996).
[40] C. Hartwigsen, S. Goedecker, and J. Hutter, Phys. Rev. B **58**, 3641 (1998).
[41] M. Krack, Theor. Chem. Acc. **114**, 145 (2005).
[42] C. Domain, R. Besson, and A. Legris, Acta Mater. **50**, 3513 (2002).
[43] P. Jelinek, H. Wang, J. P. Lewis, O. F. Sankey, and J. Ortega, Phys. Rev. B **71**, 235101 (2005).
[44] S. J. Clark, M. D. Segall, C. J. Pickard, P. J. Hasnip, M. J. Probert, K. Refson, and M. C. Payne, Z. Kristallogr. **220**, 567 (2005).

[45] S. Kenny and A. Horsfield, Comput. Phys. Commun. **180**, 2616 (2009), 40 YEARS OF CPC: A celebratory issue focused on quality software for high performance, grid and novel computing architectures.
[46] See Supplemental Material at http://link.aps.org/supplemental/10.1103/PhysRevMaterials.4.043801 for additional methodological details and supporting results, which includes Refs. [64–69].
[47] H. Wu, N. Zhang, H. Wang, and S. Hong, J. Theor. Comput. Chem. **11**, 1261 (2012).
[48] S. Han, L. A. Zepeda-Ruiz, G. J. Ackland, R. Car, and D. J. Srolovitz, Phys. Rev. B **66**, 220101(R) (2002).
[49] G. Vérité, C. Domain, C.-C. Fu, P. Gasca, A. Legris, and F. Willaime, Phys. Rev. B **87**, 134108 (2013).
[50] G. Vérité, F. Willaime, and C. C. Fu, *Solid State Phenomena*, Vol. 129 (Trans Tech Publications, Switzerland, 2007), pp. 75–81.
[51] W. M. C. Foulkes, Phys. Rev. B **48**, 14216 (1993).
[52] D. Nguyen-Manh, D. G. Pettifor, and V. Vitek, Phys. Rev. Lett. **85**, 4136 (2000).
[53] D. Nguyen-Manh, V. Vitek, and A. P. Horsfield, Prog. Mater. Sci. **52**, 255 (2007).
[54] H. J. Gotsis, D. A. Papaconstantopoulos, and M. J. Mehl, Phys. Rev. B **65**, 134101 (2002).
[55] M. J. Mehl and D. A. Papaconstantopoulos, Phys. Rev. B **54**, 4519 (1996).
[56] A. T. Paxton and C. Elsässer, Phys. Rev. B **82**, 235125 (2010).
[57] W. Ding, H. He, and B. Pan, J. Mater. Sci. **50**, 5684 (2015).
[58] P. F. Li and B. C. Pan, J. Phys.: Condens. Matter **24**, 305802 (2012).
[59] C. Z. Wang, B. C. Pan, and K. M. Ho, J. Phys.: Condens. Matter **11**, 2043 (1999).
[60] H. Haas, C. Z. Wang, M. Fähnle, C. Elsässer, and K. M. Ho, Phys. Rev. B **57**, 1461 (1998).
[61] N. Goldman, Chem. Phys. Lett. **622**, 128 (2015).
[62] J. P. Lewis, P. Jelínek, J. Ortega, A. A. Demkov, D. G. Trabada, B. Haycock, H. Wang, G. Adams, J. K. Tomfohr, E. Abad, H. Wang, and D. A. Drabold, Phys. Status Solidi B **248**, 1989 (2011).
[63] M. Boleininger, A. A. Guilbert, and A. P. Horsfield, J. Chem. Phys. **145**, 144103 (2016).
[64] G. B. Walker and M. Marezio, Acta Metall. **7**, 769 (1959).
[65] W. B. Pearson, *A Handbook of Lattice Spacings and Structures of Metals and Alloys: International Series of Monographs on Metal Physics and Physical Metallurgy*, Vol. 4 (Elsevier, Amsterdam, 2013).
[66] F. D. Murnaghan, Proc. Natl. Acad. Sci. USA **30**, 244 (1944).
[67] A. H. Larsen, J. J. Mortensen, J. Blomqvist, I. E. Castelli, R. Christensen, M. Dułak, J. Friis, M. N. Groves, B. Hammer, C. Hargus, E. D. Hermes, P. C. Jennings, P. B. Jensen, J. Kermode, J. R. Kitchin, E. L. Kolsbjerg, J. Kubal, K. Kaasbjerg, S. Lysgaard, J. B. Maronsson *et al.*, J. Phys.: Condens. Matter **29**, 273002 (2017).
[68] A. J. Morris, R. J. Nicholls, C. J. Pickard, and J. R. Yates, Comput. Phys. Commun. **185**, 1477 (2014).
[69] F. Jona and P. M. Marcus, Phys. Rev. B **66**, 094104 (2002).